JCI insight

RESEARCH ARTICLE

TLR4-dependent fibroblast activation drives persistent organ fibrosis in skin and lung

Swati Bhattacharyya,[1] Wenxia Wang,[1] Wenyi Qin,[2] Kui Cheng,[3] Sara Coulup,[3] Sherry Chavez,[3] Shuangshang Jiang,[4] Kirtee Raparia,[5] Lucia Maria V. De Almeida,[5] Christian Stehlik,[5] Zenshiro Tamaki,[1] Hang Yin,[3,4] and John Varga[1]

[1]Northwestern Scleroderma Program, Feinberg School of Medicine, Chicago, Illinois, USA. [2]Department of Bioengineering, University of Illinois at Chicago, Chicago, Illinois, USA. [3]Department of Chemistry and Biochemistry and the BioFrontiers Institute, University of Colorado Boulder, Boulder, Colorado, USA. [4]School of Pharmaceutical Sciences, Tsinghua University, Beijing, China. [5]Feinberg School of Medicine, Northwestern University, Evanston, Illinois, USA.

Persistent fibrosis in multiple organs is the hallmark of systemic sclerosis (SSc). Recent genetic and genomic studies implicate TLRs and their damage-associated molecular pattern (DAMP) endogenous ligands in fibrosis. To test the hypothesis that TLR4 and its coreceptor myeloid differentiation 2 (MD2) drive fibrosis persistence, we measured MD2/TLR4 signaling in tissues from patients with fibrotic SSc, and we examined the impact of MD2 targeting using a potentially novel small molecule. Levels of MD2 and TLR4, and a TLR4-responsive gene signature, were enhanced in SSc skin biopsies. We developed a small molecule that selectively blocks MD2, which is uniquely required for TLR4 signaling. Targeting MD2/TLR4 abrogated inducible and constitutive myofibroblast transformation and matrix remodeling in fibroblast monolayers, as well as in 3-D scleroderma skin equivalents and human skin explants. Moreover, the selective TLR4 inhibitor prevented organ fibrosis in several preclinical disease models and mouse strains, and it reversed preexisting fibrosis. Fibroblast-specific deletion of TLR4 in mice afforded substantial protection from skin and lung fibrosis. By comparing experimentally generated fibroblast TLR4 gene signatures with SSc skin biopsy gene expression datasets, we identified a subset of SSc patients displaying an activated TLR4 signature. Together, results from these human and mouse studies implicate MD2/TLR4-dependent fibroblast activation as a key driver of persistent organ fibrosis. The results suggest that SSc patients with high TLR4 activity might show optimal therapeutic response to selective inhibitors of MD2/TLR4 complex formation.

Introduction

Fibrosis, the hallmark of systemic sclerosis (SSc), is characterized by excessive production and persistent accumulation of collagens and other extracellular matrix (ECM) molecules in skin, lungs, and other internal organs. The process underlies a large number of fibrotic diseases that, in aggregate, account for a considerable proportion of deaths worldwide. With no effective therapy to date, fibrosis therefore represents a significant unmet global health need (1). The extent and activity of fibrosis in SSc varies considerably from one patient to another and over the course of the disease, but the determinants that govern this heterogeneity are largely unknown. Robust genetic associations of SSc with components of the innate immune system have been demonstrated (2). Dysregulated innate immune signaling in a genetically predisposed individual might therefore cause myofibroblasts transformation and sustained activation within lesional tissues underlying intractable organ fibrosis (3).

TLRs and related pattern-recognition receptors represent the first line of host defense against microbial pathogens (4). Cell surface receptors such as TLR4 and endosomal receptors such as TLR3 recognize extrinsic pathogen-associated molecule patterns (PAMPs) such as LPS and virus-derived nucleic acids. Significantly, TLRs also recognize damage-associated molecule patterns (DAMPs) that arise endogenously during various forms of noninfectious tissue injury (5). Endogenous TLR4 ligand DAMPs include ECM proteins such as hyaluronan, fibrinogen, tenascin-C, and fibronectin-EDA that are generated within injured

Conflict of interest: The authors declare that no conflict of interest exists.

Submitted: November 27, 2017
Accepted: May 23, 2018
Published: July 12, 2018

Reference information:
JCI Insight. 2018;3(13):e98850.
https://doi.org/10.1172/jci.insight.98850.

microenvironments, where they function as danger signals or alarmins enabling both hematopoietic and tissue-resident cells to sense and respond to damage. Regulated PAMP sensing by TLR4 has a unique requirement of myeloid differentiation 2 (MD2), an accessory receptor lacking a transmembrane domain that interacts with the extracellular domain of TLR4 to form the signaling-competent receptor (6). The requirement for MD2 as an accessory pattern-recognition receptor for PAMPs appears to be unique for TLR4 (7, 8). Whether TLR4-dependent cellular responses elicited by endogenous DAMPs similarly require MD2 remains an important unanswered question. Since dysregulated TLR4 signaling driven by aberrant generation or persistent accumulation of DAMPs is implicated in chronic inflammatory diseases, strategies to selectively inhibit TLR4 signaling promise to afford control of these conditions (5). Eritoran, a synthetic mimic of the pathogenic lipid-A domain of LPS, competes for an internal pocket of MD2 and inhibits TLR4 signaling (9). While eritoran, along with TAK-242 (resatorvid), has been evaluated in phase III sepsis trials, it failed to demonstrate clinical efficacy (10, 11). The viability of therapeutic targeting of TLR4 therefore remains to be established. Even less is known regarding the role and therapeutic potential of TLR4 blockade in chronic fibrotic conditions such as SSc.

We recently demonstrated that particular DAMPs are markedly upregulated in fibrotic skin and lungs in patients with SSc and largely colocalize with TLR4-expressing myofibroblasts (12–14). In mice, genetic ablation of either of 2 DAMPs prominently associated with SSc, fibronectin-EDA and tenascin-C, resulted in markedly attenuated skin and lung fibrosis and enhanced fibrosis resolution, suggesting a fundamental pathogenic role for DAMP-TLR4 signaling in driving persistent organ fibrosis (13, 14). Moreover, mice lacking functional TLR4 were also protected from experimentally induced fibrosis (12, 15–19). In light of these findings, the present studies were undertaken to seek evidence for altered TLR4 signaling in SSc, elucidate the role of MD2 in DAMP-dependent fibrotic responses, and assess the therapeutic potential of selective MD2/TLR4 targeting in fibrosis. Our results provide evidence for augmented MD2 and TLR4 expression and signaling in subsets of SSc skin biopsies. Selective blockade of TLR4 signaling with a potentially novel small molecule abrogated in vitro and ex vivo profibrotic responses, and it prevented and reversed organ fibrosis in multiple distinct mouse models. Furthermore, fibroblasts-specific deletion of TLR4 protected mice from fibrosis. These results establish the rationale for selective therapeutic targeting of MD2 to block pathogenic DAMP-TLR4 signaling in patients with SSc.

Results

Upregulated TLR4 and MD2 in an inflammatory intrinsic subset of SSc skin biopsies. In light of aberrant DAMP expression observed in SSc tissues (12–14), and mechanistic studies revealing a previously unsuspected role for DAMP-TLR4 activation in persistent fibrogenesis (13, 14), we sought to assess tissue levels of *TLR4* and its unique coreceptor *MD2* in SSc. To this end, we interrogated a meta-analysis of 4 distinct SSc transcriptomes (GSE9285, GSE32413, GSE45485, and GSE59785; https://www.ncbi.nlm.nih.gov/geo/) representing skin biopsies from 80 SSc patients (83% female) and 26 healthy controls. Seventy patients had diffuse cutaneous SSc (dcSSc), and 10 had limited cutaneous SSc (lcSSc). Both *TLR4* and *MD2* mRNA were significantly elevated in biopsies mapping to the inflammatory intrinsic gene subset, accounting for 50% of all SSc biopsies (*TLR4,* $P = 0.0012$ compared with controls; *MD2*, $P < 0.0001$ compared with controls) (Figure 1A). Moreover, inflammatory intrinsic gene subset biopsies were significantly enriched ($P < 0.0001$) with a previously described fibroblast LPS-responsive gene signature (Supplemental Table 1; supplemental material available online with this article; https://doi.org/10.1172/jci.insight.98850DS1) (20, 21), which itself also showed strong positive correlation with MD2 and TLR4 expression (Figure 1, C and D). Levels of *MD2* showed significant correlation with *TLR4* ($r = 0.302$, $P = 0.0079$, Spearman's correlation) (Figure 1B), as well as with the modified Rodnan Skin Score ($r = 0.27$, $P = 0.019$, Spearman's correlation). There was no significant correlation between either *TLR4* or *MD2* with patient age (*TLR4*, $r = 0.087$, $P = 0.33$; *MD2*, $r = 0.088$, $P = 0.14$).

Blockade of MD2/TLR4 association abrogates TLR4 responses in vitro and in vivo. Striking DAMP accumulation in SSc biopsies, coupled with elevated expression of TLR4 and MD2, led us to hypothesize that constitutive fibroblast activation in lesional tissues might involve a DAMP/MD2/TLR4 signaling axis. To address the viability of targeting MD2/TLR4 complex formation for inhibiting fibrosis, we searched for novel compounds to selectively block the pathway, taking advantage of the MD2 coactivator requirement unique to TLR4, but not other TLRs, for MD2 (7). High-throughput in silico screening of a drug-like library identified a pharmacologically auspicious β-amino alcohol derivative (T5342126) as a potentially

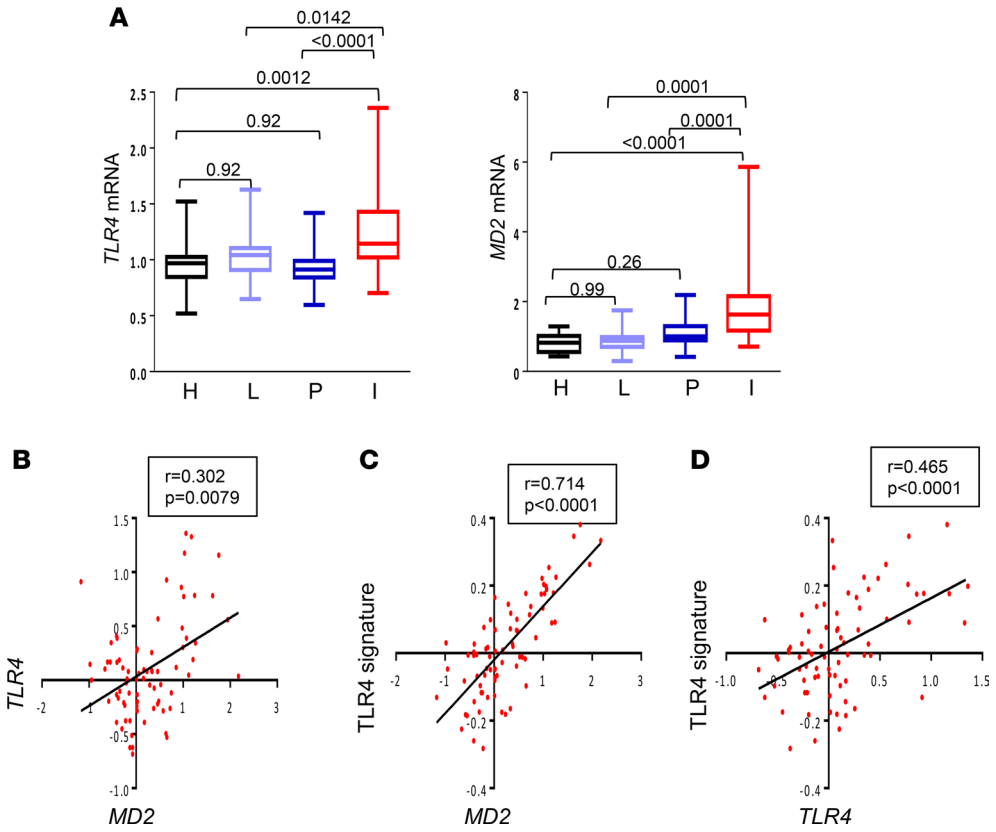

Figure 1. Upregulated TLR4 and coreceptor MD2 in SSc skin biopsies. (**A**) Expression microarray datasets (GSE9285, GSE32413, GSE45485, and GSE59785) were queried for TLR4 and MD2 levels. Results are shown as box plots (25th to 75th percentile; horizontal lines represent median, maximum, and minimum values). H, healthy; L, limited; I, inflammatory; P, diffuse proliferative intrinsic subset. One-way ANOVA followed by Sidak's multiple comparison test. (**B**) Correlation of MD2 with TLR4 levels. Each dot is a single biopsy. Spearman's rank correlation. (**C** and **D**) MD2 and TLR4 levels correlate with TLR4 signature scores (GSE24125) (20). Spearman's rank correlation.

novel TLR4 inhibitor (22–24). Based on molecular-docking stimulation, this small molecule is predicted to compete with MD2 for binding to TLR4, thus preventing formation of the signaling-competent TLR4 complex (9, 25). In preliminary experiments with normal fibroblasts, T5342126 showed no cytotoxicity in concentrations up to 50 μM (Figure 2A), while inflammatory cytokine production induced by ultra-pure LPS, but not by the TLR2 ligand Pam3Cys, was significantly attenuated by T5342126 (Figure 2B). Based on results from pilot experiments indicating that pretreatment of mice with 1 mg/kg of T5342126 significantly attenuated i.p. LPS-induced IL-6 production (Figure 2C) and peritoneal inflammation (Supplemental Figure 1), subsequent in vivo experiments used 1 mg/kg/d of inhibitor, unless otherwise indicated.

MD2/TLR4 blockade prevents and reverses skin fibrosis. The in vivo antifibrotic potential of T5342126 was first evaluated in a mouse model of bleomycin-induced fibrosis (12). At day 22 of bleomycin, a nearly 2-fold increase in the thickness of the dermis ($P < 0.05$), and marked intradermal accumulation of densely packed collagen bundles, were evident (Figure 3A). Treatment with T5342126 was accompanied by a 50% reduction in dermal thickening (Figure 3B), decreased accumulation of α-smooth muscle actin$^+$ (αSMA$^+$) dermal fibroblasts ($P < 0.05$) (Figure 3C), and reduced upregulation of profibrotic genes *Col1a1, αsma,* and *Il6* in the lesional skin (Figure 3D). To evaluate the effect of TLR4 inhibition on established fibrosis, treatment was initiated at day 15, when bleomycin-induced dermal fibrosis is already evident (14). Results showed that MD2/TLR4 inhibition reduced dermal thickness ($P < 0.01$) and enhanced collagen mRNA expression, indicating reversal of existing fibrosis (Figure 3, B and D). Separate experiments with DBA/2J mice treated with T5342126 yielded similar results in both fibrosis prevention and reversal protocols (Supplemental Figure 2). Chronic administration of T5342126 was not associated with adverse effects in either mouse strain. To determine the effect of TLR4-MD2 inhibition on cutaneous inflammation, we examined lesional skin changes at an early stage (day 7 of bleomycin). Immunostaining for CD3 and CD68 (T cell and macrophage markers, respectively) showed substantial increases in the numbers of CD3$^+$ and CD68$^+$ cells ($P < 0.05$) in

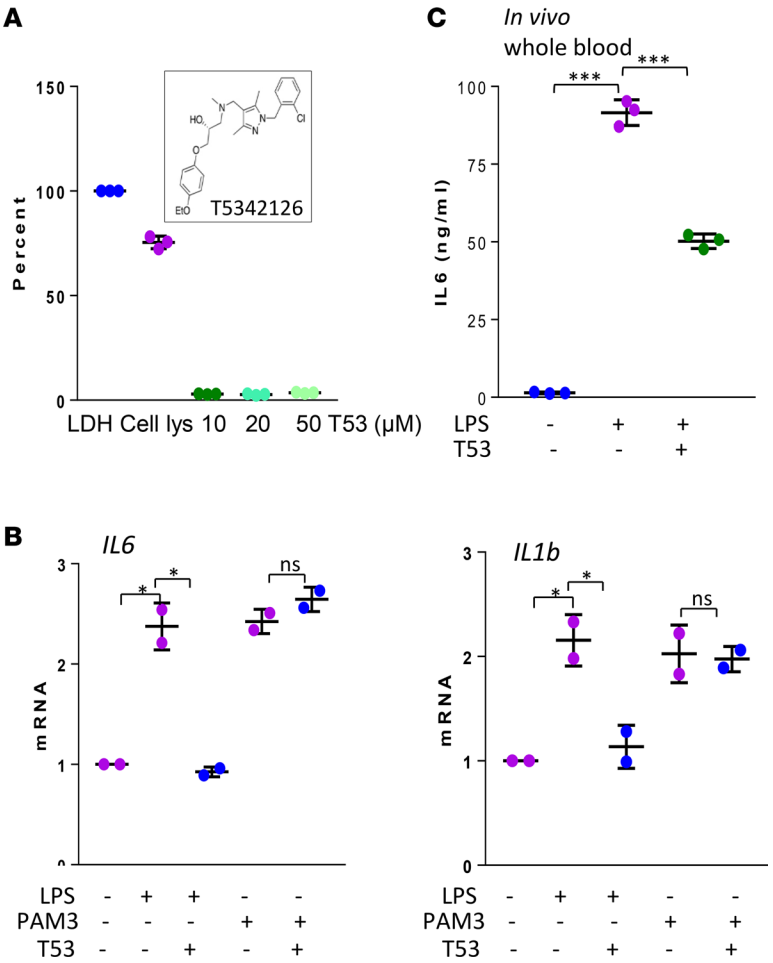

Figure 2. MD2/TLR4 inhibitor blocks LPS-induced responses. (**A** and **B**) Normal skin fibroblasts were incubated with T5342126 (10 μM or as indicated) for indicated periods. (**A**) After 24 hours, cytotoxicity was determined from triplicate determination (percent of LDH release). Inset, structure of T5342126. (**B**) Preincubation with LPS or PAM3Cys (1 μg/ml) for 1 hour followed by T5342126 treatment for 24 hours. Quantitative PCR (qPCR), normalized with GAPDH mRNA; results represent mean ± SD of triplicate determinations from 2 independent experiments. One-way ANOVA followed by Sidak's multiple comparison test. *$P < 0.05$. (**C**) C57BL/6J mice were i.p. injected with T5342126 or vehicle, followed by LPS (i.p.). At 4 hours, levels of serum IL-6 were determined by ELISA. Results are shown as mean ± SD from 3 mice. Student's *t* test. ***$P < 0.0001$.

the upper dermis, which was significantly ($P < 0.05$) attenuated in mice with concurrent T5342126 treatment (Supplemental Figure 3)**.** Double-label immunofluorescence staining indicated an increase of ~27% of myofiboblasts, and ~13% of macrophages within the lesional dermis in bleomycin-treated mice expressed TLR4 compared with PBS-treated control (Supplemental Figure 4). The proportion of both TLR4$^+$ myofibroblasts and macrophages was significantly decreased with T5342126 treatment ($P < 0.01$) Approximately 15% of increase in CD31$^+$ endothelial cells expressed TLR4 in the lesional skin was seen, and T5342126 treatment had no significant effect on this number (Supplemental Figure 4)**.**

In order to evaluate the effect of TLR4 inhibition on inflammation-independent fibrosis, we treated female TSK1/+ mice with T5342126 or vehicle initiated at 6 weeks of age, when skin fibrosis is already apparent and continued for 6 weeks (26). Vehicle-treated TSK1/+ mice displayed a substantial increase in hypodermal thickness, as reported previously (14). In contrast, TSK1/+ mice treated with T5342126 showed significantly attenuated hypodermal thickening ($P = 0.031$) (Figure 3E) and reduced *Col1a1* and *Col1a2* mRNA levels (Supplemental Figure 5). See Figure 3F for experimental schemes of Figure 3, A and E.

MD2/TLR4 blockade protects mice from peritoneal fibrosis. Long-term peritoneal dialysis is frequently complicated by peritoneal fibrosis, which can be phenocopied in mice injected with chlorhexidine gluconate (CG) (27). To explore the impact of TLR4 inhibition in peritoneal fibrosis, male C57BL/6J mice were administered CG in combination with T5342126 initiated concurrently with (preventive) or 7 days following (therapeutic) initiation of CG (Figure 4B). At day 21, the parietal peritoneal membranes showed a nearly 10-fold increase in thickness ($P < 0.01$) and marked accumulation of collagen (Figure 4A). Treatment with T5342126 was highly effective in preventing, as well as reversing, fibrosis, with 60% reduced membrane thickness, and it attenuated expression of fibrotic genes (*Col1a2*, *αsma*, *Il6* and *Tgfb1*) within the fibrotic peritoneal lining (Figure 4, A and C). Moreover, the accumulation of FSP1$^+$ and CD68$^+$ cells, as well as levels of TLR4 and phospho-p65, were significantly reduced in the

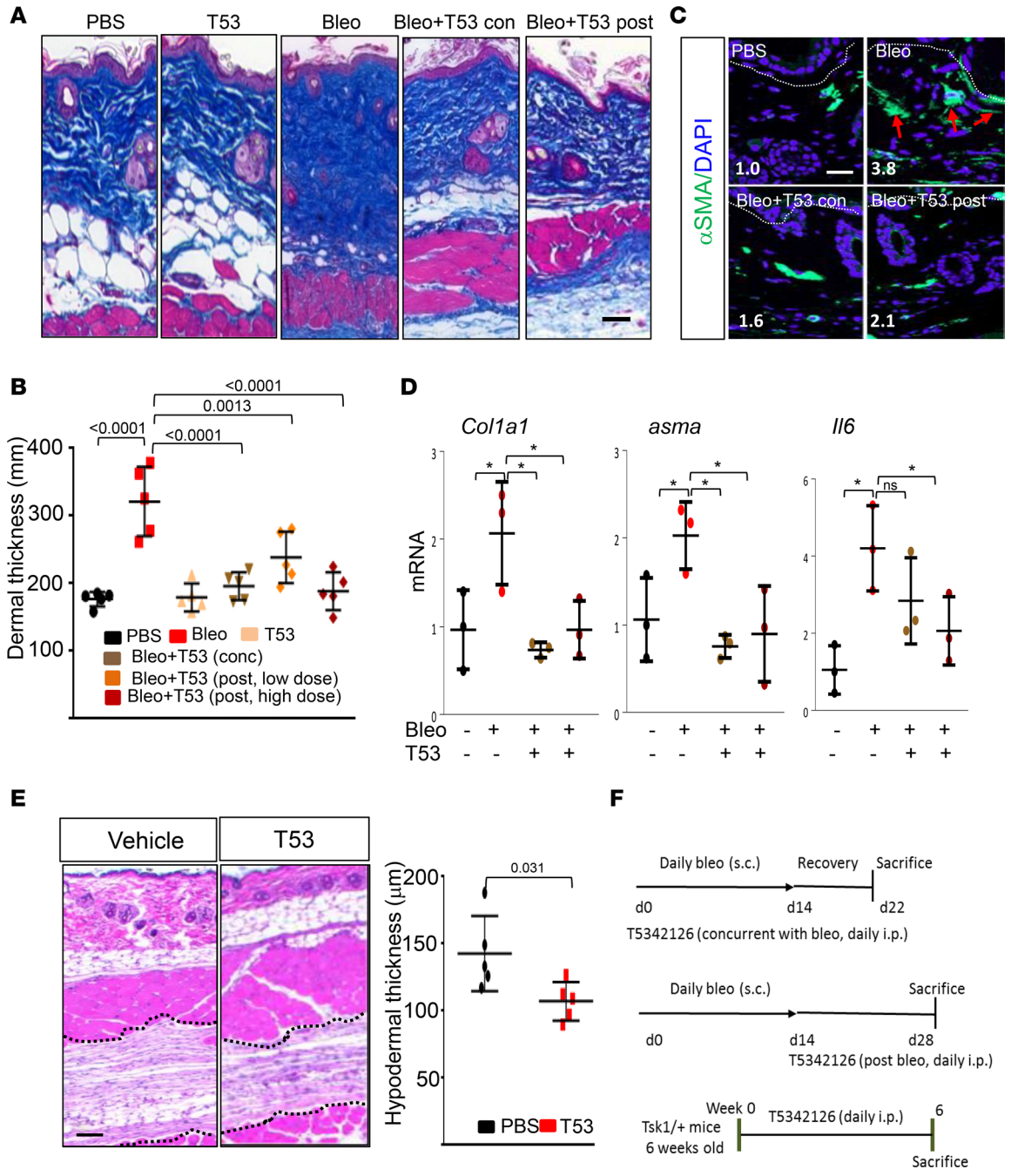

Figure 3. MD2/TLR4 inhibitor treatment ameliorates skin fibrosis. (**A–D**) C57BL/6J mice received daily s.c. injections of PBS or bleomycin alone, bleomycin together with T5342126 (0.5 or 1 mg/kg/d), or vehicle started on day 0 or day 15. Mice were sacrificed at day 22, and skin was harvested for analysis. (**A**) Masson's Trichrome stain. Representative images. Scale bar: 25 μm. (**B**) Dermal thickness (mean ± SD of 5 determinations/hpf from 5 mice/group). One-way ANOVA followed by Sidak's multiple comparison test. (**C**) Immunofluorescence using antibodies to α-smooth muscle actin (αSMA, green) and DAPI (blue). Representative images. Scale bar: 50 μm. Red arrows, α-SMA$^+$ cells in dermis. Scale bar: 200 μm. Relative fluorescence intensities (means from 4 randomly selected from 3 mice/group). (**D**) qPCR. Results, normalized with GAPDH, are mean ± SD of triplicate determinations from 3 mice/group. One-way ANOVA followed by Sidak's multiple comparison test. *$P < 0.05$. (**E**) Six-week-old Tsk1/+ mice injected with i.p. T5342126 daily were sacrificed at 12 weeks of age, and dorsal skin was harvested. Left panels, H&E stain (dotted lines indicate hypodermis); right panel, hypodermal thickness (mean ± SD of 5 determinations/hpf from 5 mice/group). Scale bar: 200 μm. Student's *t* test. (**F**) Schemes of the experiments in **A** and **E**.

lesional membrane (Figure 4D). Double-label immunofluorescence indicated an increase of ~50% of αSMA$^+$ myofibroblasts and ~20% of F4/80$^+$ macrophages in the lesional membrane expressing TLR4 in CG-treated mice compared with vehicle-treated control; their proportions were significantly attenuated with T5342126 treatment ($P < 0.01$) (Supplemental Figure 6).

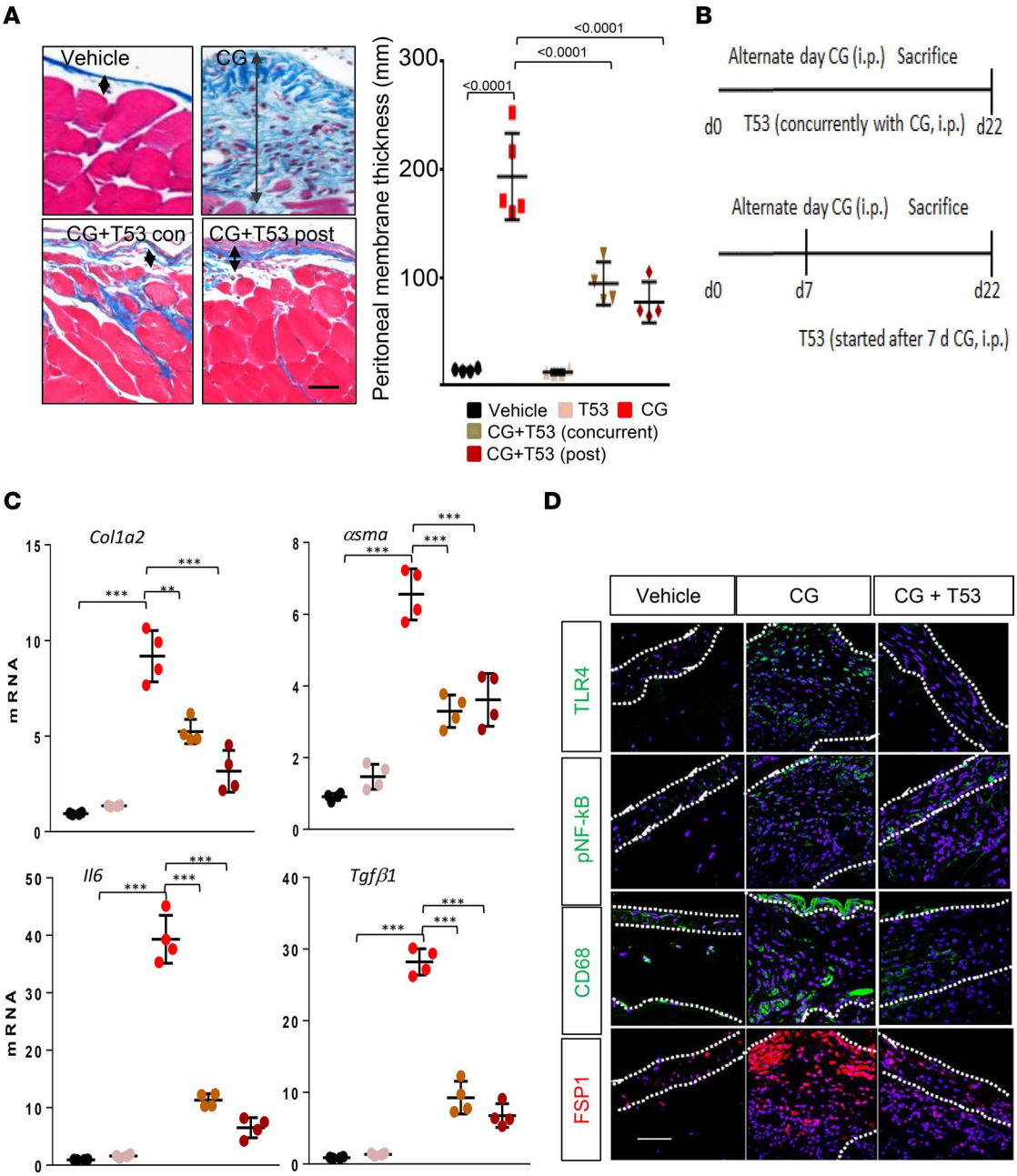

Figure 4. MD2/TLR4 inhibitor ameliorates peritoneal fibrosis. C57BL/6J mice received i.p. injections of vehicle or chlorhexidine gluconate (CG) alone (every alternate day) or together with i.p. T5342126 (1 mg/kg/d) started concurrently with, or 1 week following, initiation of CG injections. Mice were sacrificed at day 22, and parietal peritoneal membranes were harvested for analysis. (**A**) Left panel, Masson's trichrome stain, representative images. Scale bar: 25 μm. Right panel, submesothelial compact zone thickness. Results are mean ± SD of 5 determinations/hpf from 5 mice/group. One-way ANOVA followed by Sidak's multiple comparison test. (**B**) Scheme of the experiments described **A**. (**C**) Real-time qPCR. Results, normalized with GAPDH, represent the mean ± SD of triplicate determinations from 4 mice/group. One-way ANOVA followed by Sidak's multiple comparison test; $^{**}P < 0.001$, $^{***}P < 0.0001$. (**D**) Immunofluorescence using antibodies to TLR4, pNF-κB p50, CD68, or Fsp1. Representative images. Scale bar: 50 μm.

MD2/TLR4 blockade abrogates DAMP-induced ex vivo fibrotic responses. To investigate the mechanisms underlying the antifibrotic effects of T5342126 at the cellular level, we first studied adult and neonatal fibroblasts in confluent monolayers. Incubation with T5342126 abrogated the stimulation of *COL1A1*, *ASMA*, and *IL6* in a dose-dependent manner and inhibited type I collagen and αSMA expression and stress fiber incorporation elicited by either fibronectin-EDA (Fn^{EDA}) or tenascin-C, both implicated as pathogenic DAMPs in SSc (Figure 5 and Supplemental Figure 7A). To evaluate the therapeutic efficacy of T5342126 in a physiologically relevant context, we used ex vivo skin organ cultures. To induce fibrosis, explants

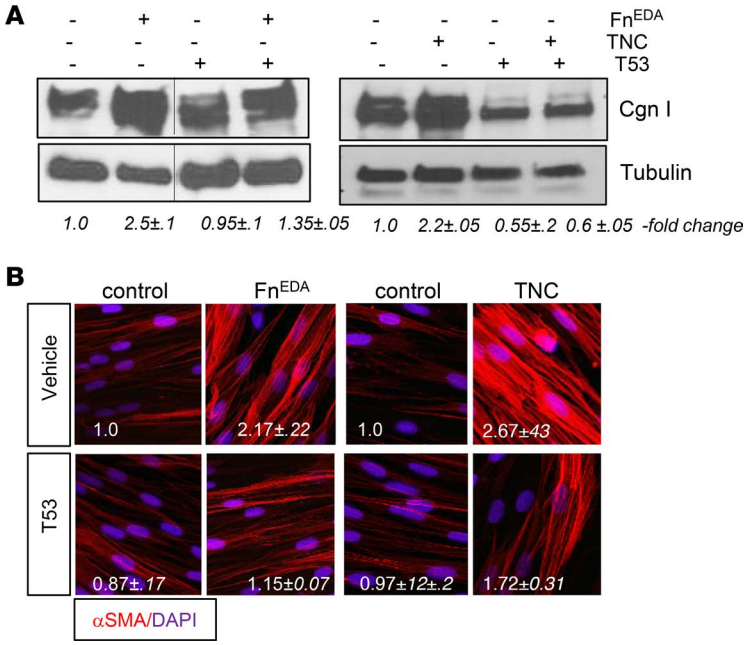

Figure 5. MD2/TLR4 inhibitor abrogates DAMP-induced profibrotic cellular responses. Confluent human skin fibroblast cultures were incubated for 72 hours with Fn^{EDA} (10 μg/ml) or tenascin-C (2 μg/ml) in media together with T5342126 or vehicle. (**A**) Immunoblots of whole cell lysates using antibodies to type I collagen. Representative immunoblots. Values indicate relative band intensities corrected for tubulin (means from 2 independent experiments). (**B**) Fibroblasts were fixed, incubated with antibodies to α-SMA or DAPI, and examined by immunofluorescence microscopy. Representative images. Original magnification, 400×. Quantification of fluorescence intensities using ImageJ (means from 4 randomly selected hpf from 2 independent experiments).

were injected with tenascin-C, along with T5342126 or vehicle; 7 or 14 days later, they were harvested for analysis. While significant increase in dermal thickness ($P < 0.0001$) and accumulation of collagen were evident in tenascin-C–injected skin (Figure 6), T5342126 prevented dermal fibrosis ($P < 0.0001$) and attenuated stimulation of profibrotic genes *COL1A1*, *COL3A1*, *IL6*, and *MCP1* (Figure 6, A, C, and D, and Supplemental Figure 7B). Second harmonic generation imaging of tenascin-C–injected skin explants confirmed that significant increase in the forward-to-backward second harmonic generation (F^{SHG}/B^{SHG}) pixel ratio (assessed as percent of fibrillar collagen–rich area with F^{SHG}/B^{SHG} pixel intensity > 1) was significantly attenuated with T5342126 treatment (Figure 6B, inset).

TLR4 inhibition mitigates the activated SSc fibroblast phenotype. To examine the cell-autonomous role of TLR4 in the persistently activated SSc fibroblast phenotype, confluent monolayers of fibroblasts from different SSc donors were incubated with T5342126 to block MD2-mediated signaling. In response, each cell line showed reduced collagen gene expression (mean = 50%, $P < 0.05$) and αSMA levels (Figure 7, A and B). Plastic dishes traditionally used in cell culture experiments present fibroblasts with supraphysiologic substrate rigidity that exerts profound influence on their behavior (28). To circumvent this concern, we used 3-dimensional (3-D) organotypic raft cultures that recapitulate the biomechanically relaxed environment of human skin (29). In 3-D skin equivalents, SSc fibroblasts progressively remodel their dermal microenvironment, with time-dependent increases in collagen deposition, matrix reorganization, accumulation of DAMPs, and substrate rigidity (13, 14). Incubation in media with T5342126 for 14 days resulted in significantly reduced rigidity ($P < 0.01$) (Figure 7C) and collagen content (Figure 7D) of these rafts.

Fibroblast-specific TLR4 ablation protects mice from fibrosis. Expression of TLR4 on either BM-derived or stromal cells might contribute to fibrotic responses elicited by DAMPs (30). To directly examine the contribution of resident fibroblasts in this process, we generated mice with fibroblast-specific *Tlr4* deletion ($TLR4^{fibcko}$) by crossing mice hemizygous for Cre ($Col1a2\text{-}Cre^{+/-}$) and homozygous for loxP-Tlr4 ($Tlr4^{fl/fl}$) (Supplemental Figure 8). Tamoxifen-treated $TLR4^{fibcko}$ mice showed no overt phenotype for up to 16 weeks of age. Selective TLR4 ablation was confirmed by Western blot analysis of explanted skin fibroblasts and BM-derived macrophages (Supplemental Figure 8, C and D). Bleomycin treatment elicited a 2-fold increase in dermal thickness ($P = 0.0001$) and collagen accumulation ($P = 0.02$) in $TLR4^{fl/fl}$ mice, while similarly treated $TLR4^{fibcko}$ mice showed significantly reduced dermal thickness ($P = 0.012$), collagen accumulation, and Col1a1 mRNA expression in the lesional skin (Figure 8). Subsequent experiments sought to explore the role of TLR4 in lung fibrosis using $TLR4^{fibcko}$. S.c. bleomycin elicited prominent lung changes with an influx of inflammatory cells, an emergence of fibrotic foci that were primarily subpleural in localization, substantial collagen accumulation, and architectural features of fibrosis (Figure 8C). Masson's trichrome staining and hydroxyproline assays confirmed increased collage accumulation in the lungs.

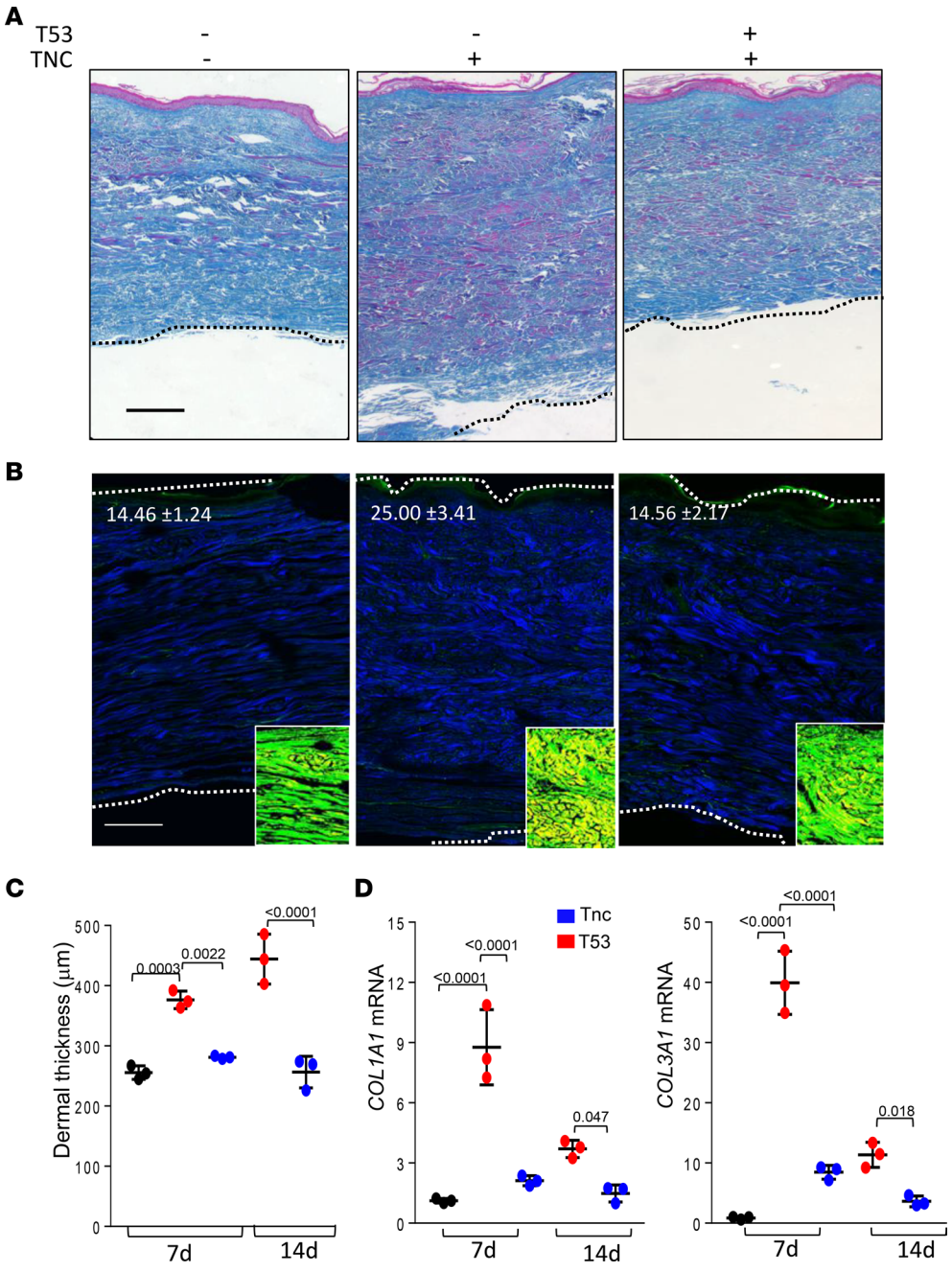

Figure 6. MD2/TLR4 inhibitor attenuates fibrotic responses in human skin explants. Human skin explants were injected with tenascin-C (2 μg/ml) together with vehicle or T5342126 (10 μM) on alternating days for up to 14 days. At indicated intervals, tissues were harvested for analysis. (**A**) Trichrome stain; representative images. Scale bar: 100 μm. (**B**) SHG imaging on unstained tissue. The F^{SHG}/B^{SHG} ratios were calculated to assess collagen microstructure. Collagen fibrils, blue; background, green. Values inside panels represent percent of collagen-rich area (F^{SHG}/B^{SHG} pixel intensity > 1, as shown in yellow in inset). Scale bar: 150 μm. (**C**) Thickness of dermis (mean ± SD of 5 determinations from at least 3 explants [47 ± 5 years; female]). One-way ANOVA followed by Sidak's multiple comparison test. (**D**) qPCR. Results, normalized with GAPDH, are mean ± SD of triplicate determinations from 3 explants per experimental group. One-way ANOVA followed by Sidak's multiple comparison test.

Each of these markers of pulmonary fibrosis showed substantial attenuation in *TLR4*^{fibcko} mice (Figure 8, C and D). Moreover, lung fibroblasts explanted from *TLR4*^{fibko} mice showed complete loss of tenascin-C–induced fibrotic responses (Figure 8E).

Fibroblast TLR4 gene signatures in SSc skin biopsies. To assess TLR4-induced fibroblast responses at the genome-wide level, low-passage primary skin fibroblasts were transfected with constitutively active TLR4 or empty vector, and 24 hours later, the whole cell lysates were prepared for luciferase assays and Western blot analysis. Ectopic TLR4 expression resulted in dose-dependent increase in NF-κB-luc activity, indicating active TLR4 signaling (Figure 9A). Next, 3 independent cultures of skin fibroblasts were transfected with TLR4 for 24 hours, and total RNA was processed for hybridizations to Illumina Human HT-12 microarray chips containing > 48,000 probes. Analysis of the data demonstrated that TLR4 induced a broad spectrum of gene expression changes in fibroblasts. Biological triplicates showed comparable changes in gene expression patterns (Figure 9B). At 24 hours, TLR4 induced differential expression of 872 genes ($P < 0.01$; FDR < 0.01), with 332 showing upregulation and 540

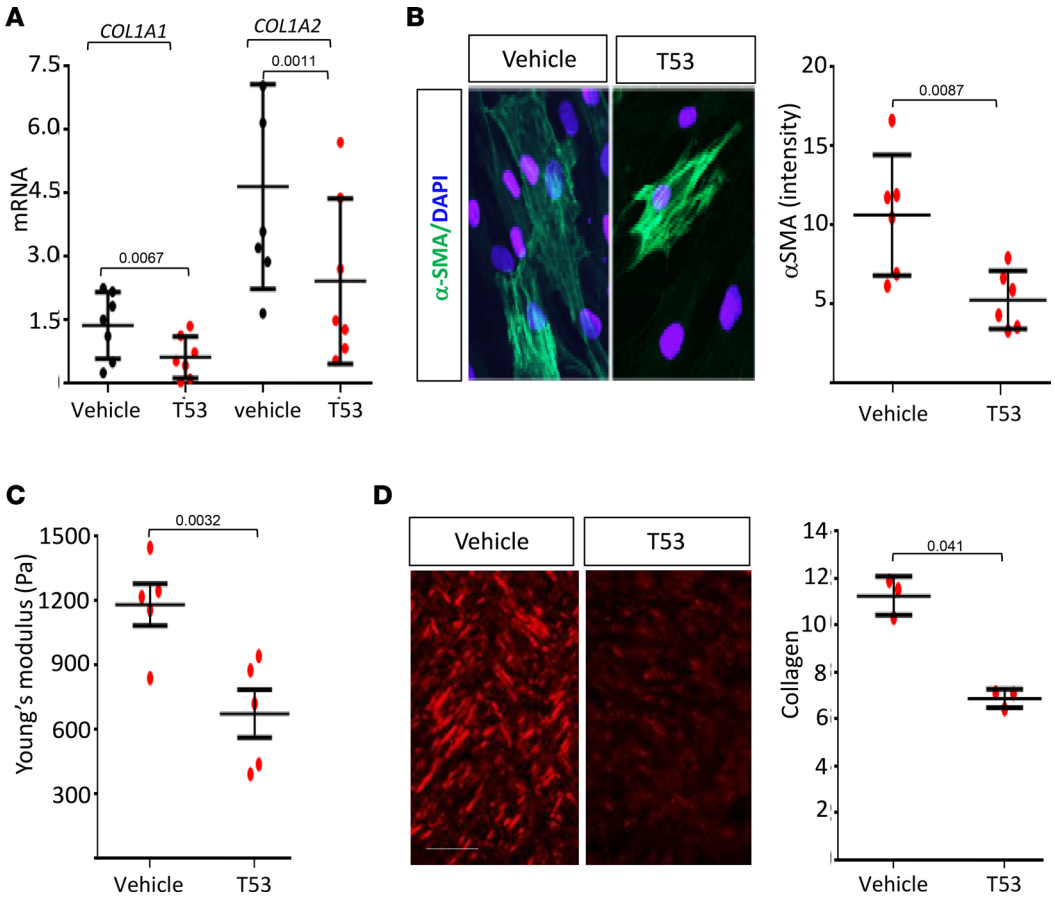

Figure 7. MD2/TLR4 inhibitor attenuates the activated SSc fibroblast phenotype. (**A**) Confluent cultures of early-passage SSc skin fibroblasts were incubated in media with T5342126 (10 μM) or vehicle, and harvested after 24 hours. qPCR. Results, normalized with GAPDH, are mean ± SD of inhibition compared with vehicle-treated controls (100%). (**B**) SSc skin biopsies were immunolabeled using antibodies to αSMA (green). Left panel, representative immunofluorescence images. Original magnification, 400×. Right panel, quantification of immunofluorescence. Results are mean ± SD from 4 randomly selected hpf/slide. Mann-Whitney *U* test. (**C** and **D**) Three-dimensional human skin equivalents populated with SSc fibroblasts were incubated in media with T5342126 or vehicle for 10 days and harvested for analysis. (**C**) Dermal compartment stiffness. Results expressed as Young's modulus represent the mean ± SD of 12 independent determinations from each of 3 SSc fibroblasts. Mann-Whitney *U* test. (**D**) Left panel, Picrosirius red stain. Representative images; scale bar: 10 μm. Right panel, quantitation of intensity. Bars represent the mean± SD from 6 randomly selected hpf/raft from 3 separate rafts constitute with different SSc fibroblasts. Mann-Whitney *U* test.

downregulation. Gene Ontology (GO) analysis revealed significant enrichment ($P = 1 \times 10^{-8}$) of functional groups related to response to cytokines and organic substance, apoptosis, defense, cell migration, wound healing, ECM organization, and vascular development (Supplemental Table 3).

To determine the potential clinical significance of activated TLR4 signaling in SSc, we sought to measure the TLR4-responsive gene signature (defined as the set of 332 genes upregulated in response to TLR4, GSE79621) in a microarray dataset comprising 27 skin biopsies (GSE9285). A heatmap was generated using 112 active probes (variance cutoff of 0.1, representing 102 unique genes) as described in Methods (Figure 9C, upper panel). Hierarchical clustering stratified the biopsies into the previously described diffuse-proliferative and inflammatory gene expression subsets (31, 32). Inflammatory intrinsic subset biopsies (Figure 9C, lower panel), accounting for ~34% of all SSc biopsies in the present study, showed significant enrichment with the TLR4-responsive gene signature (Pearson correlation = 0.2) compared with other biopsy subsets (2 samples, 2-tailed *t* test, $P < 0.001$) (33). Analysis of a replication microarray dataset comprising 28 skin biopsies from an independent cohort of 15 dcSSc patients (GSE32413) (32) confirmed significantly higher TLR4-responsive gene signatures in biopsies mapping to the inflammatory intrinsic subset (comprising 50% of all SSc biopsies; average Pearson correlation = 0.1, *t* test $P < 0.05$) (Supplemental Figure 9).

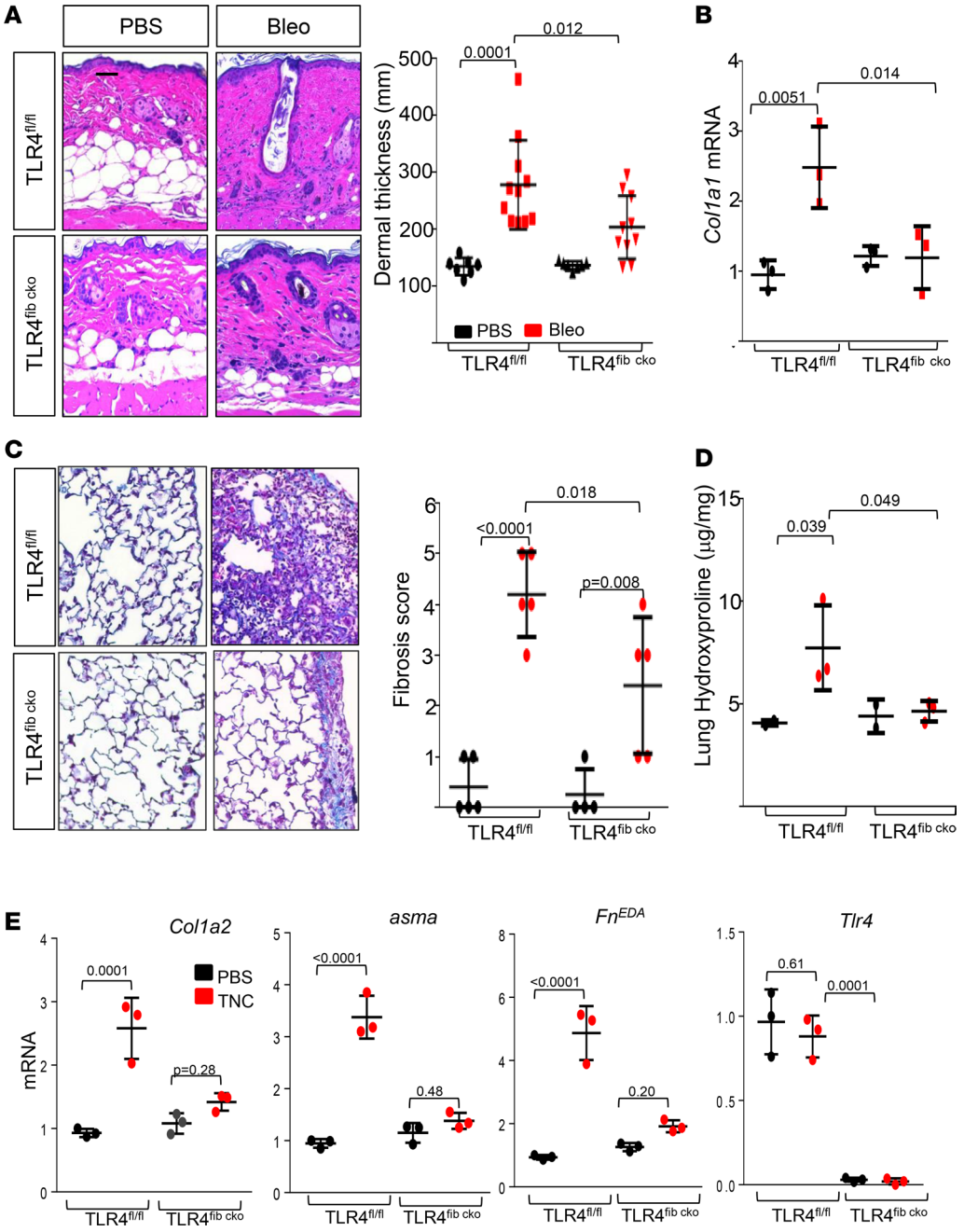

Figure 8. Fibroblast-specific TLR4 ablation ameliorates organ fibrosis. (**A–D**) *TLR4*$^{fl/fl}$ mice and *TLR4*^{fibcko} mice in parallel received bleomycin or PBS via daily s.c. injection for 2 weeks (5 days/week) and were sacrificed on day 22. Lesional skin (**A** and **B**) and lungs (**C** and **D**) were harvested for analysis. (**A**) Left panel, H&E stain; representative images. Original magnification, 100×. Right panel, dermal thickness (mean ± SD of 5 determinations/hpf from at least 7 mice). (**B**) qPCR. Results, normalized with GAPDH, are mean ± SD of triplicate determinations from 3 mice per group. One-way ANOVA followed by Sidak's multiple comparison test. (**C**) Left panel, Masson's trichrome stain; representative images. Scale bar: 100 µm. Right panel, fibrosis score; each dot represents the mean ± SD of 5 independent determinations from 5 mice per group. One-way ANOVA followed by Sidak's multiple comparison test. (**D**) Collagen content. Each dot represents mean ± SD from triplicate determination from 3 mice per group. One-way ANOVA followed by Sidak's multiple comparison test. (**E**) Lung fibroblasts explanted from *TLR4*$^{fl/fl}$ mice and *TLR4*^{fibcko} mice in parallel were incubated at confluence in media with tenascin-C (2 µg/ml) for 24 hours. qPCR. Results, normalized with GAPDH, are mean ± SD of triplicate determinations. One-way ANOVA followed by Sidak's multiple comparison test.

Discussion

Persistent fibroblast activation underlies unresolving skin and lung fibrosis in SSc and represents a major barrier to effective therapy. While immune cells within lesional tissue are prominent in early-stage disease, chronic fibrosis is largely pauci-inflammatory, indicating a role for immune cell-independent factors in maintaining the activated state of fibroblasts (34). In particular, DAMPs generated within the fibrotic

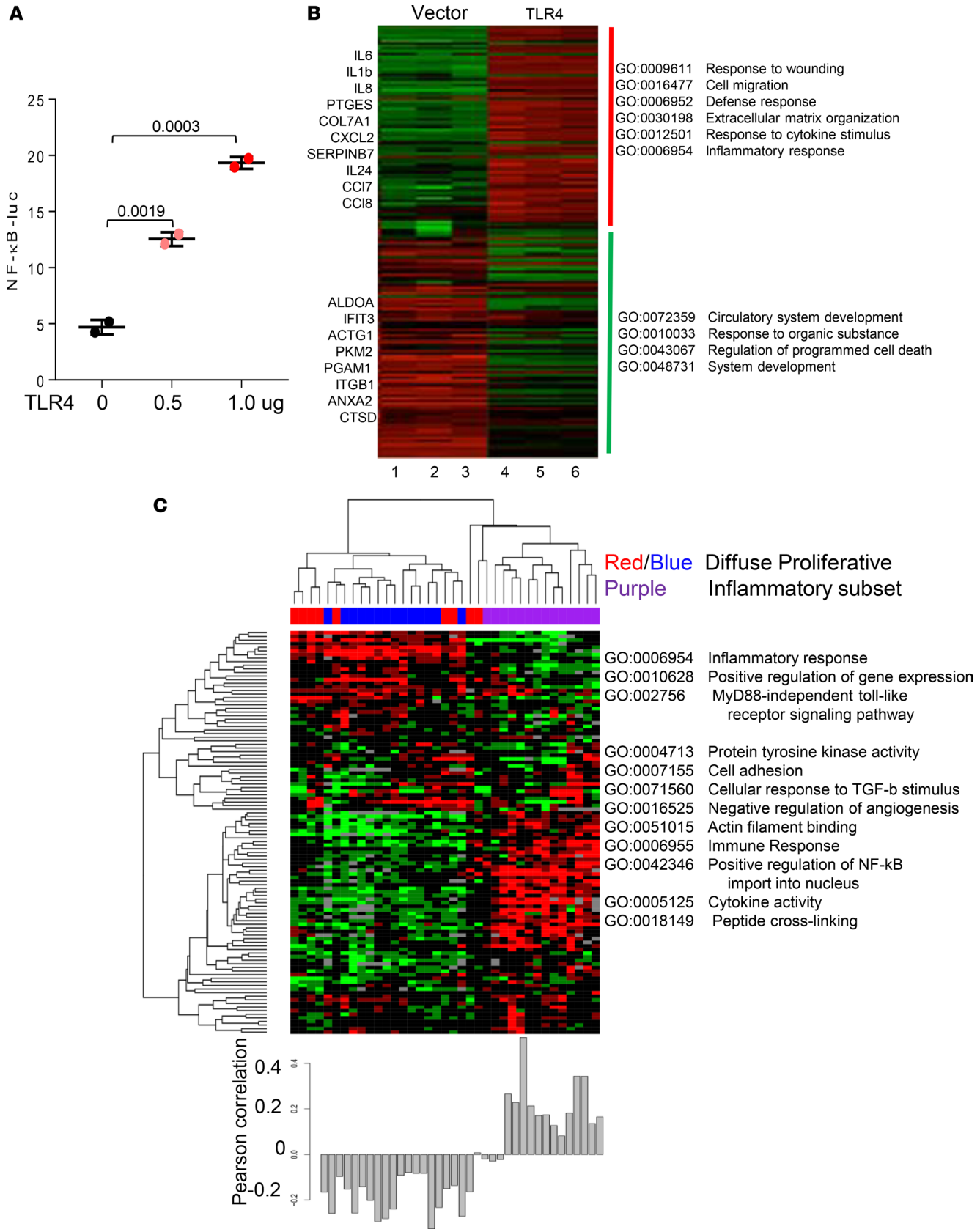

Figure 9. TLR4-response gene signature scores in SSc skin biopsies. To generate a TLR4 responsive gene signature, normal skin fibroblasts were transiently transfected with constitutively active TLR4 or empty vector alone or in combination with NF-κB-luc. Forty-eight hours later, cultures were harvested. (**A**) Lysates were assayed for their luciferase activities; results are mean ± SD of triplicate determinations from 2 separate experiments. (**B**) Analysis of TLR4-regulated gene expression (FDR = 0.05; fold change ≥ 1.5). RNA was isolated and hybridized to Illumina human HT-12 version 4 Expression Microarray Chips (GSE79621).

Heatmaps showing fold change compared with the average in control (empty vector). Red, increased; green, decreased. Most highly represented Gene Ontology (GO) terms for each cluster are shown to the right. Lane 1–3, empty vector; 4–6, TLR4. (**C**) Experimentally derived TLR4 signature in SSc skin biopsies (GSE9285). Heatmap shows hierarchical clustering of the dataset generating diffuse and inflammatory intrinsic subsets. Clustering was performed with 246 probes representing 176 unique TLR4 regulated genes at an FDR of 5% showing ≥ 1.5-fold change from the above experiment. Color coding indicate intrinsic subset designations. Most highly represented GO terms shown next to each cluster (right). Pearson's correlation of the TLR4-responsive gene signature in each biopsy specimen is shown below heatmap.

milieu might be sensed by stromal cell MD2 and elicit TLR4 activation, resulting in transformation into myofibroblasts and secretion of ECM molecules that are, themselves, endogenous TLR4 ligands. Thus, tissue damage begets a self-amplifying cycle of fibrosis mediated through the MD2/TLR4 complex and its endogenous DAMP ligands. Blocking the generation of DAMPs, or their recognition by MD2/TLR4 on resident stromal cells, might represent novel approaches to promote fibrosis resolution.

Deregulated TLR signaling is implicated in chronic inflammatory diseases, autoimmunity, and cancer (35). While TLRs are best characterized on BM-derived cells of the immune system, they are also expressed in tissue-resident stromal cells, where they play key roles in tissue homeostasis and repair, but also contribute to the persistence of sterile inflammatory responses underlying chronic diseases (34). Uniquely among the surface TLRs, TLR4 activation by LPS and other exogenous ligands requires accessory receptor MD2 (6). Endogenous TLR4 ligands encompass structurally diverse molecules released by dying or damaged cells such as high-mobility box 1 (HMGB1) and heat shock proteins (HSPs); self-nucleic acids, including single- and double-stranded DNA; RNA; mitochondrial DNA; and nucleic acid-antibody complexes or are generated de novo in response to injury. Prominent among the endogenous TLR4 ligand danger signals are the ECM molecules hyaluronan, tenascin-C, and alternatively spliced fibronectin EDA isoforms. These oncofetal variant proteins show high levels of tissue expression during embryonic development, but they are largely absent from most tissues in healthy adults and appear only transiently during normal wound healing (5). Persistent DAMP accumulation is a hallmark of cancer and chronic inflammatory and fibrotic conditions. We have shown previously that both fibronectin-EDA and tenascin-C are markedly upregulated and colocalize with activated myofibroblasts in skin and lung biopsies from patients with SSc (12–14). Furthermore, these DAMPs have the capacity to stimulate the expression of ECM genes and promote myofibroblast transformation, cell migration, and mechanical force generation in mesenchymal cells (34). The present studies indicate that TLR4 and MD2 were markedly upregulated in a subset of SSc skin biopsies; and levels showed a strong correlation with the TLR4 gene signature within the same biopsies. Additionally, we found prominent expression of an experimentally derived fibroblast TLR4-responsive gene signature, composed of genes implicated in both inflammation and wound healing, in a subset of SSc skin biopsies. Taken together, these findings implicate ongoing MD2/TLR4 activation driven by endogenous TLR4 ligand DAMPs in driving persistent fibrotic responses.

In view of the pathogenic role of TLR4 in multiple chronic diseases, substantial effort is directed at the development of potent TLR4 inhibitors. The small molecule TLR4 antagonists Eritoran and TAK-242 failed to demonstrate efficacy in Phase III clinical trials of sepsis (10, 11). Using a combination of virtual screening and medicinal chemistry, we recently identified potentially novel β-amino alcohol derivatives that selectively suppress TLR4-dependent cellular responses by disrupting the MD2/TLR4 complex (22). Here, we show that treatment with T5342126 prevented and reversed fibrosis in multiple disease models. Taken together with previous findings (14), these observations indicate that endogenous TLR4 ligands generated during sterile injury elicit and maintain fibrotic responses in both inducible and genetic (spontaneous) forms of tissue fibrosis. Significantly, blocking MD2/TLR4 complex formation reversed established fibrosis, consistent with the notion that fibrosis maintenance requires ongoing TLR4-dependent fibroblast activation (14). We had shown previously that TLR4 activation by elicited by either LPS or endogenous TLR4 ligands elicit fibrotic responses, and synergizes with TGF-β, in a variety of mesenchymal cells (12, 13). While TLR4 repressed the antifibrotic miR29, as well as the endogenous TGF-β antagonist BAMBI, the precise mechanisms underlying the profibrotic effects of TLR4 activation remain to be elucidated (12). The present results indicate that targeting the TLR4-MD2 complex resulted in inhibition of proinflammatory as well as profibrotic responses elicited by endogenous DAMPs or occurring spontaneously in SSc fibroblasts.

Disease heterogeneity is a hallmark of SSc and contributes to the lack of effective therapies, to date (36). Molecular profiling of SSc skin biopsies has identified stable and reproducible intrinsic gene expression subsets (31, 32). A subset of SSc biopsies showed robust upregulation of genes associated

with innate immune signaling despite a paucity of immune cells, suggesting that inflammatory gene signatures might originate from resident stromal cells. Indeed, using an experimentally derived fibroblast TLR4-responsive gene signature to interrogate SSc skin biopsies, we found that biopsies displaying a TLR4 gene signature mapped to the inflammatory intrinsic gene subset. Fibroblast TLR4 signatures might therefore represent tissue biomarkers of ongoing TLR4 activity and have potential utility for identifying SSc patients potentially responsive to TLR4 inhibition. Comparison of experimentally generated TLR4-responsive gene signatures in monocytes vs. skin fibroblasts showed partial overlap of differentially expressed genes (hypergeometric test; $P = 0.02$). Only the fibroblast TLR4 gene signature showed significant enrichment with wound healing, matrix organization, and TGF-β signaling pathways. Further supporting the pathogenic role of fibroblast TLR4, fibroblast-specific ablation was found to protect mice from development and persistence of cutaneous and pulmonary fibrosis. While these findings reveal important disease-relevant differences in how fibroblasts vs. monocytes respond to TLR4 stimulation, and support a previously unrecognized inflammation-independent pathogenic role of fibroblast TLR4 signaling, the role of TLR4 in fibrosis is cell type, organ, and injury specific. For example, while pulmonary fibrosis induced by either LPS or s.c. bleomycin was ameliorated in mice lacking TLR4 (18, 37), intratracheal bleomycin-induced acute lung injury was also reported to be exacerbated in TLR4-null mice, due to impaired alveolar epithelial cell regeneration (38, 39).

Together, our results provide evidence that cellular MD2/TLR4 signaling elicited by tenascin-C and related DAMPs plays a pathogenic role in persistent fibrosis in SSc. A potentially novel small molecule selectively targeting MD2/TLR4 prevented DAMP-dependent fibrotic responses in mesenchymal cells and prevented — as well as reversed — organ fibrosis in a variety of disease models and mouse strains. Other TLR4 inhibitors working via mechanisms distinct from those of T5342126 have been previously shown to target fibroblast activation (12, 14). In light of the unique MD2 coreceptor requirement of TLR4, but not other TLRs, targeting MD2 might represent a novel and distinct therapeutic strategy for selective disruption of pathogenic DAMP-TLR4 signaling. Protein-protein interaction have been conventionally regarded as daunting drug targets due to the difficulty of disrupting the expansive protein interfaces using synthetic agents with molecular weight <500 daltons. Our approach represents a unique, first-in-its-class chemical probe to test the druggability of the clinicallly relevant protein complex, circumventing conventional TLR4 inhibition approaches that have proven ineffective in clinical trials. Further lead optimization, coupled with transcriptome-based selection of SSc patients demonstrating ongoing TLR4 activity, might therefore provide entirely new opportunities for safe and effective targeted therapy of SSc and other persistent fibrosing conditions.

Methods

Cell culture and reagents. Primary cultures of human fibroblasts were established by explantation from neonatal foreskin or from forearm kin biopsies of patients with SSc or healthy controls (14). Low-passage fibroblasts were grown either in monolayers in plastic dishes and studied at early confluence, or they were embedded into collagen plugs used to create 3-D organotypic human skin equivalents, as we described (12, 29, 40). Lung fibroblasts from neonatal *TLR4*$^{fl/fl}$ and TLR4^{fibcko} mice were established by explantation and studied at early passage in parallel. Cultures were maintained in DMEM supplemented with 10% FBS (Thermo Fisher Scientific), 1% vitamin solutions, and 2 mM L-glutamine (Lonza). All other tissue culture reagents were from Lonza. For experiments, cultures were placed in serum-free media containing 0.1% BSA (MilliporeSigma) with or without indicated concentrations of the TLR4 inhibitor T5342126 (22). The inhibitor was added 60 minutes prior to Fn^{EDA} (1 μg/ml) isolated and purified from embryonic IMR90 fibroblasts (13) or to tenascin-C (2 μg/ml, MilliporeSigma, catalog CC0651) purified from the human U251glioma cell line (14).

Preparation of T5342126. The amino alcohol derivative T5342126 was synthesized as previously reported (22, 25). All reactions were performed in oven-dried or flame-dried glassware under a dry nitrogen or argon atmosphere. Flash chromatography was performed using 32–64 μm silica gel. ^{1}H nuclear magnetic resonance (^{1}H NMR) spectra were recorded at 500 MHz in $CDCl_3$ using residual $CHCl_3$ (7.26 ppm) as the internal standard. ^{13}C NMR spectra were recorded at 75 MHz in $CDCl_3$ using residual $CHCl_3$ (77.23 ppm) as an internal reference. Exact mass was determined using electrospray ionization.

Cytotoxicity assays. Cell death or cytotoxicity was evaluated by quantification of plasma membrane damage using LDH Cytotoxicity Assay Kit II (Biovision).

Isolation and analysis of RNA. At the end of the experiments, total RNA was isolated and reverse transcribed to cDNA using Supermix (cDNA Synthesis Supermix; Quanta Biosciences) as described (12). Amplification products (50 ng) were amplified using SYBR Green PCR Master Mix (Applied Biosytems) on an Applied Biosystems 7500 Prism Sequence Detection System. Data were normalized to GAPDH RNA, and fold change in samples was calculated (14). Sequences of the primers are shown in Supplemental Table 4.

Western blot analysis. At the end of the experiments, cultures were harvested, whole cell lysates were prepared, and equal amounts of proteins (20–50 μg/lane) were subjected to Western blot analysis using primary antibodies specific for type I collagen (catalog 1310-01; Southern Biotechnology) and tubulin (catalog 1310-0, MilliporeSigma), followed by appropriate secondary antibodies (14). Membranes were then subjected to enhanced chemiluminescence detection using ECL Reagent (Pierce). Band intensities were quantitated using ImageJ (NIH) software and corrected for tubulin in each lane.

Transient transfection assays. Subconfluent fibroblast cultures were cotransfected with NF-κB-luc, constitutively active TLR4, and Renilla luciferase pRL-TK plasmids (Promega) using Superfect reagent (Qiagen). Cultures were harvested following a 24-hour incubation, and whole cell lysates were assayed for their luciferase activities (12). The experiment was performed in triplicate and repeated twice with consistent results.

Immunofluorescence confocal microscopy. To assess T5342126 modulation of fibroblast responses elicited by Fn^{EDA} or tenascin-C by immunocytochemistry, fibroblasts were incubated on 8-well Lab-Tek II chamber glass slides (Nalgene Nunc International) in serum-free DMEM supplemented with 0.1% BSA containing Fn^{EDA} (1 μg/ml) or tenascin-C (2 μg/ml) in the absence or presence of T5342126 for up to 72 hours. In selected experiments, SSc or matched healthy fibroblasts were treated with T5342126 for 24 hours. Cells were then fixed, permeabilized, and incubated with antibodies to αSMA (catalog A5228; MilliporeSigma) at 1:100 or 1:500 dilution, followed by Alexa Fluor–labeled secondary antibodies (Invitrogen). Nuclei were identified using DAPI. Subcellular distribution of immunofluorescence was evaluated under an immunofluorescence microscope or Zeiss UV Meta 510 confocal microscope or a Nikon C2 or A1Si confocal microscope and quantitated using ImageJ (12, 33).

Bioluminescence imaging. To examine the efficacy of T5342126 in vivo, mice were pretreated with T5342126 (1 mg/kg/mouse), followed 60 minutes later by i.p. injection with ultrapure LPS-EB (Invivogen). Four hours later, luminol (100 ml/kg/mouse) was injected i.p., and in vivo bioluminescence imaging (BLI), a measure of neutrophil myeloperoxidase activity, was performed using IVIS Spectrum In Vivo Imaging System (Perkin Elmer) 10 minutes after injection with a 5-minute exposure on anesthetized mice and quantified with the Living Image software (Perkin Elmer).

Experimental models of fibrosis. A series of complementary fibrosis models (Supplemental Table 2) were employed to evaluate pharmacological TLR4 blockade in vivo. First, 8-week-old female C57BL/6J or DBA/2J mice (The Jackson Laboratory) mice received s.c. injections of bleomycin (10 mg/kg/day) or PBS daily for 5 or 10 days, along with T5342126 (0.5 or 1.0 mg/kg) by daily i.p. injections starting concurrently with bleomycin, and sacrificed on day 7 or day 22, respectively. Another group of mice received T5342126 injections starting at day 7 of bleomycin treatment and continued until sacrifice at day 28. A third group of mice received PBS, and a fourth received bleomycin alone. All treatment groups consisted of at least 5 mice, and experiments were repeated 3 times with consistent results. In a complementary noninflammatory fibrosis model, 6-week-old Tsk1/+ mice (C57BL/6J background) received T5342126 (1 mg/kg) injections i.p. daily until sacrifice at 12 weeks.

To create mice with fibroblasts-specific TLR4 deletion, mice carrying tamoxifen-inducible Cre-recombinase (*Cre-ER^T*), under the control of a fibroblast-specific 6-kb far-upstream transcriptional enhancer from the mouse COL1A2 gene (The Jackson Laboratory), were crossed with mice homozygous *TLR4$^{fl/fl}$* (with *loxP* sites on either side of exon 3 of the targeted *Tlr4* gene) from Dr. Christopher Karp (Cincinnati Children's Hospital), COL1A2-Cre-ER^T which generated *COL1A2-Cre$^{+/-}$;TLR4$^{fl/fl}$* homozygous mice (Supplemental Figure 8, C and D). The resulting offspring will have exon 3 deleted in Cre-expressing fibroblasts. Mice were genotyped with specific PCR primers. At 3 weeks of age, female *COL1A2-Cre$^{+/+}$ TLR4$^{fl/fl}$* mice were injected with 1 mg/mouse tamoxifen (MilliporeSigma, T176) or corn oil i.p. daily for 10 days (5 days/week) followed a week later by s.c. bleomycin (10 mg/kg/day) or PBS given daily for 10 days (5 days/week) (Supplemental Figure 4). Mice were sacrificed on day 22, and lesional skin and lungs were harvested for analysis.

Paraffin-embedded tissue sections (4 μm) were stained with H&E or Masson's trichrome. Thickness of the dermis, defined as the distance from the epidermal-dermal junctions to the dermal-adipose junction, or

(in TSK1/+ mice) to the loose connective tissue subjacent to the panniculus carnosus, was determined at 5 randomly selected sites as described (14). For immunofluorescence analyses, paraffin-embedded skin sections were incubated with primary rabbit antibodies against αSMA (1:100), (catalog ab5694; Abcam), followed by Alexa Fluor–labeled rabbit secondary antibodies. Nuclei were detected using DAPI. Slides were evaluated in a blinded manner under a Zeiss UV Meta 510 confocal microscope (13). Paraffin-embedded sections were incubated with primary rabbit antibodies against CD3 (catalog ab5690) and CD68 (catalog ab955) (both from Abcam; 1:100), followed by Alexa Fluor–labeled rabbit or mouse secondary antibodies. Double immunofluorescence staining using antibodies against TLR4 (catalog ab13867; Abcam, 1:50), α-SMA (catalog A5228; MilliporeSigma, 1:500), CD31 (catalog sc-1506; from Santa Cruz Biotechnology Inc., 1:100) or F4/80 (clone BM8; eBioscience, 1:100) was performed, followed by incubation with Alexa Fluor–conjugated IgG secondary antibodies (Invitrogen). Immunopositive cells in 4 randomly selected hpf from each slide were counted by a blinded observer. Sections were imaged using a Nikon A1R laser scanning confocal microscope. Tissue collagen content was determined by hydroxyproline assays using Colorimetric Assay Kits (Biovision).

Peritoneal fibrosis was induced by alternate-daily i.p. injections of 0.1% CG (Wako Pure Chemical Industries) dissolved in 15% ethanol/PBS every other day. C57BL/6J male mice (~25 g) received CG alone or received it together with i.p. T5342126 (1 mg/kg) or vehicle starting either concurrently with, or 1 week following, initiation of CG injection. At day 21, mice were sacrificed, and peritoneal tissues were carefully dissected. To avoid damage to the peritoneum, injections were made at the caudal part of the peritoneum, while the rostral portion of the parietal membrane was taken for analysis.

Peritoneal membrane thickness (submesothelial compact zone superficial to the abdominal wall muscles) was determined. Paraffin-embedded sections were incubated with primary rabbit antibodies against FSP1 (catalog 07-2274; MilliporeSigma, 1:500) and TLR4 (catalog ab13867), p-NF-kBp50 (catalog ab86299), and CD68 (catalog ab955) (all from Abcam; 1:100), followed by Alexa Fluor–labeled rabbit or mouse secondary antibodies. Nuclei were detected using DAPI. Slides were mounted and immunofluorescence was evaluated under a Zeiss UV Meta 510 confocal microscope.

ELISA. Eight-week-old female C57BL/6J mice (The Jackson Laboratory) were pretreated with vehicle or 1 mg/kg T5342126 (i.p.) for 120 minutes and were injected with LPS (10 mg/kg, i.p.). Four hours later, serum was collected and IL-6 was measured by ELISA (R&D Systems).

TLR4 blockade in ex vivo models of human skin. To evaluate the effects of TLR4 inhibition on fibrogenesis in physiologically relevant contexts, we used both human skin explants and 3-D organotypic skin equivalents. In the first approach, abdominal skin tissue obtained from cosmetic surgery was cut into 1 × 1 cm pieces that were incubated in DMEM (Corning) with 10% FBS (Thermo Fisher Scientific) with epidermis exposed to air. Skin explants were injected with tenascin-C (2 μg/ml in a total volume of 50 μl) along with T5342126 (10 μM) or vehicle every other day for up to 14 days. At indicated intervals, skin surrounding the injection site was harvested for analysis. Paraffin-embedded sections (4 μm) were stained with Masson's trichrome, and thickness of the dermis was determined at 5 randomly selected sites. SHG microscopy, which reveals changes in collagen microstructure, was used to evaluate collagen fiber organization. Unstained 22 μm–thick tissue sections were imaged for F^{SHG} and B^{SHG} signals using a multiphoton microscope (Nikon A1R MP+ Multiphoton), providing 2-photon (2P) excitation (41). The F^{SHG}/B^{SHG} pixel ratio was calculated to assess relative differences in fibrillar collagen microstructure (assessed as percent of collagen-rich area with F^{SHG}/B^{SHG} pixel intensity > 1).

In other experiments, the effect of TLR4 inhibition was evaluated using 3-D organotypic raft cultures constructed to recapitulate the topography and biochemical properties of human skin (29). Briefly, low-passage fibroblasts (300,000 cells/ml) from SSc (n = 3) or healthy control skin biopsies were resuspended in a buffered solution of rat tail type I collagen (4 mg/ml, from BD Biosciences) and seeded in 12-well cell culture plates (1.5 ml/well). Collagen plugs were allowed to polymerize for 30 minutes. Primary human epidermal keratinocytes (200,000 cells/ml) isolated from a pool (n = 3) of neonatal foreskins were seeded on top of the dermal collagen plugs and incubation-continued media supplemented with EGF (5 ng/ml) as previously described (14). Forty-eight hours later, skin equivalents were transferred to metal grids and incubated in media with T5342126 (10 μM) or vehicle up to 18 days. Rafts were then harvested, fixed in 10% neutral buffered formalin, and embedded in paraffin for picrosirius red staining. Stiffness of the dermal compartments was determined using a parallel-plate rheometer, and Young's modulus was calculated using US 200 software (Anton Paar Co.) as described (13).

Genomewide expression profiling and data analysis. To examine genomewide fibroblast responses induced by TLR4, subconfluent cultures were transfected with TLR4 or empty vector, and following

a 24-hour incubation, RNA was isolated using RNeasy mini kits (Qiagen). RNA integrity was determined using Agilent Bioanalyzer (Agilent Technologies), and labeled cDNA was hybridized to Illumina human HT12 v4 Expression Microarray Chips, as previously described (12). Raw signal intensities for each probe were obtained using Illumina Bead version 2 studio data analysis software and imported to the Bioconductor lumi package for data transformation and normalization (GSE79621). Probes with all samples absent (near or below background levels) were filtered. Stringent statistical criteria were used to identify differentially expressed genes with raw $P < 0.01$ and FDR-adjusted $P < 0.05$.

Bioinformatics analysis of TLR4 responsive gene signature. An experimentally derived TLR4 responsive gene signature was defined based on the list of genes showing ≥ 1.5-fold upregulation (FDR < 0.05) compared with controls. To measure the TLR4 gene signature in SSc, this signature was mapped to the probe representing the same gene in 2 publicly available SSc microarray datasets (GSE9285 and GSE32413). Each probe's expression value was centered to the median value across all patient samples. In order to measure the signature, probes with a variance <0.1 were excluded from further analysis. An average linkage hierarchical clustering of active probes was performed on patient samples using uncentered Pearson's correlation coefficient between the mapped probes' fold change in vitro and their median-adjusted expression values for each patient sample to measure the signature activation. All analyses and heatmap visualizations were carried out using R (http://www.r-project.org/).

Statistics. Data are presented as mean ± SD. Two-tailed Student's *t* test or Mann Whitney *U* test were used for comparisons between 2 groups. Differences among groups were examined for statistical significance using 1-way ANOVA, followed by Bonferroni or Sidak's correction. A *P* value less than 0.05 denoted the presence of statistically significant difference. Data were analyzed using Graph Pad prism (Graph Pad Software version 5, Graph Pad Software Inc.).

Study approval. Animal studies were conducted in accordance with NIH guidelines for the care and use of laboratory animals and approved by the IACUC of the Northwestern University. Studies involving human subjects were approved by the IRB of the Northwestern University, and participants provided written informed consent.

Author contributions

SB, HY, and JV conceived the project, designed experiments, and interpreted data. SB and JV wrote the manuscript. WW, ZT, SB, KC, S. Coulup, SJ, S. Chavez, LMVDA, and WQ performed the preparation of T5342126, major experiments, data acquisition, and analysis. HY and CS contributed to reagents/materials/analysis tools and critical reading of the manuscript. KR performed lung histological and pathological analyses and interpretation of the results. SB, ZT, and WQ performed statistical analysis.

Acknowledgments

We are grateful to members of the Scleroderma Research Laboratory, the staffs of the Mouse Histology & Phenotyping Laboratory (MHPL), the Northwestern University Skin Diseases Research Core, and Constandina Arvanitis (Imaging Core) for excellent technical support. This work was supported by grants from the NIH National Institute of Arthritis and Musculoskeletal and Skin Diseases (AR42309), National Institute of General Medicine (GM127003), National Natural Science Foundation of China (21572114 and 21621003), and the Scleroderma Foundation.

Address correspondence to: Swati Bhattacharyya or John Varga, Division of Rheumatology, Northwestern University Feinberg School of Medicine, 240 E. Huron Street, Chicago, Illinois 60611, USA. Phone: 312.503.0377; Email: s-bhattacharyya@northwestern.edu (S. Bhattacharyya); j-varga@northwestern.edu (J. Varga). Or to: Hang Yin, School of Pharmaceutical Sciences,Tsinghua University, Beijing, 100082, China. Phone: 86.10.6278.6251; Email: yin_hang@tsinghua.edu.cn.

1. Wynn TA, Ramalingam TR. Mechanisms of fibrosis: therapeutic translation for fibrotic disease. *Nat Med*. 2012;18(7):1028–1040.
2. Terao C, et al. Transethnic meta-analysis identifies GSDMA and PRDM1 as susceptibility genes to systemic sclerosis. *Ann Rheum Dis*. 2017;76(6):1150–1158.
3. Bhattacharyya S, Wei J, Varga J. Understanding fibrosis in systemic sclerosis: shifting paradigms, emerging opportunities. *Nat Rev Rheumatol*. 2011;8(1):42–54.
4. Kawai T, Akira S. The role of pattern-recognition receptors in innate immunity: update on Toll-like receptors. *Nat Immunol*.

2010;11(5):373–384.
5. Piccinini AM, Midwood KS. DAMPening inflammation by modulating TLR signalling. *Mediators Inflamm*. 2010:672395.
6. Carpenter S, O'Neill LA. Recent insights into the structure of Toll-like receptors and post-translational modifications of their associated signalling proteins. *Biochem J*. 2009;422(1):1–10.
7. Kim HM, et al. Crystal structure of the TLR4-MD-2 complex with bound endotoxin antagonist Eritoran. *Cell*. 2007;130(5):906–917.
8. Shimazu R, et al. MD-2, a molecule that confers lipopolysaccharide responsiveness on Toll-like receptor 4. *J Exp Med*. 1999;189(11):1777–1782.
9. Li J, Csakai A, Jin J, Zhang F, Yin H. Therapeutic Developments Targeting Toll-like Receptor-4-Mediated Neuroinflammation. *ChemMedChem*. 2016;11(2):154–165.
10. Opal SM, et al. Effect of eritoran, an antagonist of MD2-TLR4, on mortality in patients with severe sepsis: the ACCESS randomized trial. *JAMA*. 2013;309(11):1154–1162.
11. Rice TW, et al. A randomized, double-blind, placebo-controlled trial of TAK-242 for the treatment of severe sepsis. *Crit Care Med*. 2010;38(8):1685–1694.
12. Bhattacharyya S, et al. Toll-like receptor 4 signaling augments transforming growth factor-β responses: a novel mechanism for maintaining and amplifying fibrosis in scleroderma. *Am J Pathol*. 2013;182(1):192–205.
13. Bhattacharyya S, et al. FibronectinEDA promotes chronic cutaneous fibrosis through Toll-like receptor signaling. *Sci Transl Med*. 2014;6(232):232ra50.
14. Bhattacharyya S, et al. Tenascin-C drives persistence of organ fibrosis. *Nat Commun*. 2016;7:11703.
15. Seki E, et al. TLR4 enhances TGF-beta signaling and hepatic fibrosis. *Nat Med*. 2007;13(11):1324–1332.
16. Pulskens WP, et al. TLR4 promotes fibrosis but attenuates tubular damage in progressive renal injury. *J Am Soc Nephrol*. 2010;21(8):1299–1308.
17. Campbell MT, et al. Toll-like receptor 4: a novel signaling pathway during renal fibrogenesis. *J Surg Res*. 2011;168(1):e61–e69.
18. Takahashi T, et al. Amelioration of tissue fibrosis by toll-like receptor 4 knockout in murine models of systemic sclerosis. *Arthritis Rheumatol*. 2015;67(1):254–265.
19. Saigusa R, et al. Multifaceted contribution of the TLR4-activated IRF5 transcription factor in systemic sclerosis. *Proc Natl Acad Sci USA*. 2015;112(49):15136–15141.
20. Johnson ME, et al. Experimentally-derived fibroblast gene signatures identify molecular pathways associated with distinct subsets of systemic sclerosis patients in three independent cohorts. *PLoS One*. 2015;10(1):e0114017.
21. Rubins KH, Hensley LE, Relman DA, Brown PO. Stunned silence: gene expression programs in human cells infected with monkeypox or vaccinia virus. *PLoS One*. 2011;6(1):e15615.
22. Chavez SA, et al. Development of β-amino alcohol derivatives that inhibit Toll-like receptor 4 mediated inflammatory response as potential antiseptics. *J Med Chem*. 2011;54(13):4659–4669.
23. Yin H, Hamilton AD. Strategies for targeting protein-protein interactions with synthetic agents. *Angew Chem Int Ed Engl*. 2005;44(27):4130–4163.
24. Bevan DE, et al. Selection, Preparation, and Evaluation of Small- Molecule Inhibitors of Toll-Like Receptor 4. *ACS Med Chem Lett*. 2010;1(5):194–198.
25. Wang X, et al. Morphine activates neuroinflammation in a manner parallel to endotoxin. *Proc Natl Acad Sci USA*. 2012;109(16):6325–6330.
26. Weingärtner S, et al. Pomalidomide is effective for prevention and treatment of experimental skin fibrosis. *Ann Rheum Dis*. 2012;71(11):1895–1899.
27. Sakai N, Chun J, Duffield JS, Wada T, Luster AD, Tager AM. LPA1-induced cytoskeleton reorganization drives fibrosis through CTGF-dependent fibroblast proliferation. *FASEB J*. 2013;27(5):1830–1846.
28. Hinz B, et al. Recent developments in myofibroblast biology: paradigms for connective tissue remodeling. *Am J Pathol*. 2012;180(4):1340–1355.
29. Simpson CL, Kojima S, Getsios S. RNA interference in keratinocytes and an organotypic model of human epidermis. *Methods Mol Biol*. 2010;585:127–146.
30. Bhattacharyya S, Varga J. Emerging roles of innate immune signaling and toll-like receptors in fibrosis and systemic sclerosis. *Curr Rheumatol Rep*. 2015;17(1):474.
31. Milano A, et al. Molecular subsets in the gene expression signatures of scleroderma skin. *PLoS One*. 2008;3(7):e2696.
32. Pendergrass SA, Lemaire R, Francis IP, Mahoney JM, Lafyatis R, Whitfield ML. Intrinsic gene expression subsets of diffuse cutaneous systemic sclerosis are stable in serial skin biopsies. *J Invest Dermatol*. 2012;132(5):1363–1373.
33. Fang F, et al. Toll-like Receptor 9 Signaling Is Augmented in Systemic Sclerosis and Elicits Transforming Growth Factor beta-Dependent Fibroblast Activation. *Arthritis Rheumatol*. 2016;68(8):1989–2002.
34. Bhattacharyya S, Midwood KS, Yin H, Varga J. Toll-Like Receptor-4 Signaling Drives Persistent Fibroblast Activation and Prevents Fibrosis Resolution in Scleroderma. *Adv Wound Care (New Rochelle)*. 2017;6(10):356–369.
35. Awasthi S. Toll-like receptor-4 modulation for cancer immunotherapy. *Front Immunol*. 2014;5:328.
36. Varga J, Hinchcliff M. Connective tissue diseases: systemic sclerosis: beyond limited and diffuse subsets? *Nat Rev Rheumatol*. 2014;10(4):200–202.
37. He Z, Zhu Y, Jiang H. Inhibiting toll-like receptor 4 signaling ameliorates pulmonary fibrosis during acute lung injury induced by lipopolysaccharide: an experimental study. *Respir Res*. 2009;10:126.
38. Liang J, et al. Hyaluronan and TLR4 promote surfactant-protein-C-positive alveolar progenitor cell renewal and prevent severe pulmonary fibrosis in mice. *Nat Med*. 2016;22(11):1285–1293.
39. Yang HZ, et al. TLR4 activity is required in the resolution of pulmonary inflammation and fibrosis after acute and chronic lung injury. *Am J Pathol*. 2012;180(1):275–292.
40. Getsios S, et al. Desmoglein 1-dependent suppression of EGFR signaling promotes epidermal differentiation and morphogenesis. *J Cell Biol*. 2009;185(7):1243–1258.
41. Kottmann RM, et al. Second harmonic generation microscopy reveals altered collagen microstructure in usual interstitial pneumonia versus healthy lung. *Respir Res*. 2015;16:61.